Materials Today Bio 25 (2024) 101011

Contents lists available at ScienceDirect

Materials Today Bio

journal homepage: www.journals.elsevier.com/materials-today-bio

Biomimetic fabrication of sr-silk fibroin co-assembly hydroxyapatite based microspheres with angiogenic and osteogenic properties for bone tissue engineering

Yunfei Liu [a,b], Chengji Shi [a], Piaoye Ming [b,c], Lingling Yuan [a,b], Xueyu Jiang [b,c], Min Jiang [a,b], Rui Cai [b,d], Xiaorong Lan [b,d], Jingang Xiao [a,b,c,d,**], Gang Tao [b,d,*]

[a] Department of Oral and Maxillofacial Surgery, The Affiliated Stomatological Hospital, Southwest Medical University, Luzhou, 646000, China
[b] Luzhou Key Laboratory of Oral & Maxillofacial Reconstruction and Regeneration, Luzhou, 646000, China
[c] Department of Oral Implantology, The Affiliated Stomatological Hospital, Southwest Medical University, Luzhou, 646000, China
[d] Institute of Stomatology, Southwest Medical University, Luzhou, 646000, China

ARTICLE INFO

Keywords:
Silk fibroin
Strontium
Microsphere
Angiogenesis
Osteogenesis

ABSTRACT

Bone defects caused by trauma, tumor resection, or developmental abnormalities are important issues in clinical practice. The vigorous development of tissue engineering technology provides new ideas and directions for regenerating bone defects. Hydroxyapatite (HAp), a bioactive ceramic, is extensively used in bone tissue engineering because of its excellent osteoinductive performance. However, its application is challenged by its single function and conventional environment-unfriendly synthesis methods. In this study, we successfully "green" synthesized sr-silk fibroin co-assembly hydroxyapatite nanoparticles (Sr-SF-HA) using silk fibroin (SF) as a biomineralized template, thus enabling it to have angiogenic activity and achieving the combination of organic and inorganic substances. Then, the rough composite microspheres loaded with Sr-SF-HA (CS/Sr-SF-HA) through electrostatic spraying technology and freeze-drying method were prepared. The CCK-8 test and live/dead cell staining showed excellent biocompatibility of CS/Sr-SF-HA. Alkaline phosphatase (ALP) staining, alizarin red staining (ARS), immunofluorescence, western blotting, and qRT-PCR test showed that CS/Sr-SF-HA activated the expression of related genes and proteins, thus inducing the osteogenic differentiation of rBMSCs. Moreover, tube formation experiments, scratch experiments, immunofluorescence, and qRT-PCR detection indicated that CS/Sr-SF-HA have good angiogenic activity. Furthermore, *in vivo* studies showed that the CS/Sr-SF-HA possesses excellent biocompatibility, vascular activity, as well as ectopic osteogenic ability in the subcutaneous pocket of rats. This study indicates that the construction of CS/Sr-SF-HA with angiogenic and osteogenic properties has great potential for bone tissue engineering.

1. Introduction

Bone defects caused by trauma, injury, or tumor resection seriously influence the physical and mental health of patients. Traditionally, autogenous bone transplantation is regarded as the gold standard for bone defect restoration [1,2]. However, this method has some problems, such as the limited transplantation source and the risk of postoperative complications [3]. In recent years, through the integration of new knowledge and techniques in materials science, biology, and medicine, bone tissue engineering has made great progress and is one of the most promising methods for repairing bone defects [4,5]. Bone defect reconstruction is an elaborate biological process involving the interaction of complex biological events, including neuron formation, early angiogenesis, and osteogenic differentiation [6]. In the initial stages of bone defect repair, neovascularizations can deliver oxygen, nutrients, and biological factors to the defective area, thus promoting bone tissue regeneration [7,8]. Therefore, the ideal tissue engineering material for regenerating bone defects should achieve functional vascularization and

* Corresponding author. Luzhou Key Laboratory of Oral & Maxillofacial Reconstruction and Regeneration, The Affiliated Stomatological Hospital, Southwest Medical University, Luzhou, 646000, China.
** Corresponding author. Department of Oral and Maxillofacial Surgery, The Affiliated Stomatological Hospital, Southwest Medical University, Luzhou, 646000, China.
E-mail addresses: xiaojingang@swmu.edu.cn (J. Xiao), taogang@swmu.edu.cn (G. Tao).

https://doi.org/10.1016/j.mtbio.2024.101011
Received 15 December 2023; Received in revised form 5 February 2024; Accepted 26 February 2024
Available online 27 February 2024

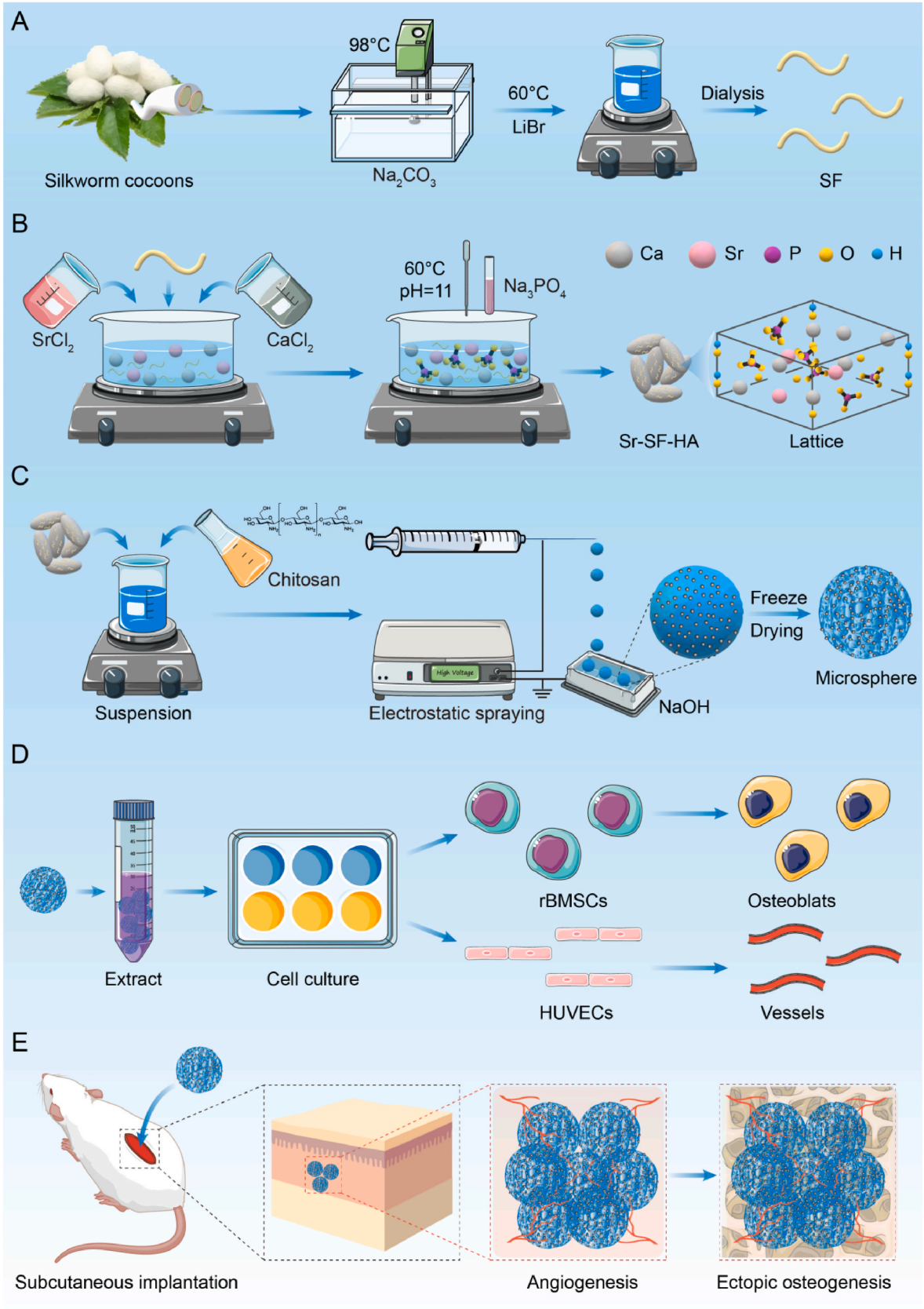

Fig. 1. A schematic illustration of the preparation and application of CS/Sr-SF-HA. (A) Preparation of silk fibroin powder. (B) Synthesis of Sr-SF-HA. (C) Preparation of CS/Sr-SF-HA. (D) CS/Sr-SF-HA application in promoting osteogenesis and angiogenesis *in vitro*. (E) CS/Sr-SF-HA application in promoting ectopic osteogenesis and angiogenesis *in vivo*.

bone regeneration [2].

Hydroxyapatite (HAp) is a bioactive ceramic with good biological activity, biocompatibility, and bone conductivity. More importantly, HAp has the same chemical structure as the inorganic components of human bone tissue, and it can be absorbed and utilized by bone tissue. Therefore, it is widely used to prepare bone tissue engineering materials [9,10]. Strontium (Sr) and calcium (Ca) have similar physical and chemical properties and are both essential trace elements that participate in the processes of bone mineralization. They play a significant role in adjusting the structure and intensity of human bones. *In vitro* and *in vivo* studies have shown that strontium-containing biomaterials can induce osteogenic differentiation of mesenchymal stem cells while inhibiting the formation of osteoclasts [11–14]. In addition, Xing M et al. found that strontium can promote angiogenesis in endothelial cells and repair infarcted hearts, suggesting strontium is a critical element in promoting vascular development and osteogenic differentiation [15]. Therefore, partially substituting calcium in hydroxyapatite with strontium may yield multifunctional composite hybrid materials with excellent angiogenic and osteogenic properties.

HAp nanocrystals is a major part of the inorganic material of the bone extracellular matrix, and together with organic components, including collagen and lipids, form the extracellular matrix of bone [16]. So, bone tissue engineering biomaterials consisting of organic and inorganic substances can simulate the structure of the bone extracellular matrix, which may bring higher bone regeneration potential [17,18]. Many natural compounds have been used as templates for the growth of HAp and for preparing bone tissue engineering biomaterials with induced osteogenic activity [13]. In recent years, the use of proteins as an organic template for preparing hydroxyapatite nanocrystals has received much attention as it avoids the introduction of toxic and harmful chemical reagents. In addition, researchers find that HAp nucleation starts from binding anionic side chains in proteins to calcium ions [19–22]. Therefore, with the increase of protein and acidic amino acid, HAp nucleation is promoted [23]. Silk fibroin (SF), the natural macromolecular fibrin derived from silk, which possesses excellent biodegradability and biocompatibility, is widely used in the biomedical fields of drug delivery, wound dressings, artificial blood vessels, and bone tissue scaffolds [24]. Interestingly, the composite of HAp and SF can enhance biocompatibility, promote osteogenesis, and even reduce the inflammation of sterile implanted biomaterials *in vivo* [23,25–28]. Therefore, we plan to select SF as the organic mineralization template for the deposition of strontium-substituted hydroxyapatite (Sr-HAp) and to use the chemical co-precipitation-hydrothermal method to green prepare Sr-SF-HA.

Local direct implantation of Sr-SF-HA particles may result in rapidly losing efficacy, and the quick release of ions in a short time may cause more damage than benefits to tissues. The loading of Sr-SF-HA particles into carriers such as 3D scaffolds, hydrogels, fibrous membranes, and microspheres can solve this problem perfectly, achieving a slow release of functional substances [11,12]. Compared with other carriers, microspheres can meet the repair requirements of irregular and complex shape bone defects. And microspheres can be implanted into the lesion site through minimally invasive implantation. Moreover, the excellent drug delivery properties of microspheres enable prolonged drug release [29]. In addition, the microspheres supply a high specific surface area, facilitating the effective transfer of nutrients and the sustained release of functional substances to achieve better therapeutic results [30,31]. These advantages have attracted increasing attention in the biomedical field, and microspheres are widely used in bone, cartilage, periodontium, and skin tissue repair [23,32–34]. Microspheres prepared from natural polymers such as gelatine, chitosan, dextran, cellulose, and synthetic polyesters such as polylactic acid and polylactic acid-ethanolic acid have been widely used. Among them, chitosan (CS), a product of the natural polysaccharide chitin, is an ideal material for the preparation of microspheres because of its good biodegradability and biocompatibility [35–37].

In this study, we first successfully extracted SF solution from silkworm cocoons (Fig. 1A) and synthesized Sr-SF-HA in a green way using SF as the template (Fig. 1B). TEM showed that Sr-SF-HA were nano-rod structures with HAp characteristic lattice spacing, such as (002) and (211). XRD revealed the characteristic diffraction peaks of Sr-SF-HA with HAp crystals at (002), (210), (211), (300), (202), (310), (222), and (213). Then, the rough composite microspheres loaded with Sr-SF-HA were prepared through electrostatic spraying technology and freeze-drying method (Fig. 1C). The diameter of CS/Sr-SF-HA was 409.4 ± 84.5 μm, and Sr-SF-HA were uniformly distributed in microspheres. CCK-8 assays and live/dead staining demonstrated excellent biocompatibility of microspheres. The results of ALP, ARS, qRT-PCR, immunofluorescence, and western blotting showed that the CS/Sr-SF-HA had good osteogenic induction ability. Scratch assay, tube formation test, qRT-PCR, and immunofluorescence detection indicated that the CS/Sr-SF-HA could promote angiogenesis (Fig. 1D). Furthermore, the CS/Sr-SF-HA were implanted into the subcutaneous pocket of rats to detect the ability to promote angiogenesis and ectopic osteogenesis *in vivo* (Fig. 1E). The expression of CD31, COL-1, and OCN was upregulated in the CS/Sr-SF-HA treatment group, indicating that the microspheres have good osteogenic and angiogenic abilities. By systematically evaluating the osteogenesis and angiogenesis of microspheres, we aim to develop a new biomaterial for treating bone defects.

2. Experimental section

2.1. Materials

Calcium chloride ($CaCl_2$), strontium chloride ($SrCl_2$), Sodium phosphate (Na_3PO_4), Lithium bromide (LiBr), and chitosan were obtained from Aladdin Biochemical Technology Co., LTD (Shanghai, China). Sodium hydroxide (NaOH) was purchased from Kelong Chemicals Co., LTD (Chengdu, China). Silkworm cocoons were obtained from the Seri Cultural Research Institute (Jiangsu, China). All other chemical reagents such as BCIP/NBT alkaline phosphatase color development kit (Beyotime, China), α-modified Eagle's medium (α-MEM; Gibco, USA), Cell Counting Kit-8 (CCK-8, Beyotime, China), high-glucose Dulbecco's modified Eagle's medium (High Glucose DMEM; Gibco, USA), Live/Dead® Viability Kit (Thermo Fisher Scientific, USA), Matrigel (Corning, USA) and alizarin red staining solution (ARS, Cyagen, China) were purchased from commercial sources.

2.2. Preparation of silk fibroin solution

Firstly, put the silkworm cocoons into 2% (w/v) Na_2CO_3 solution at 98°C for 30 min, then wash with ddH_2O three times to remove the sericin and leave the silk fibroin [38]. Next, dissolved the silk fibroin in 9.3 M LiBr aqueous solution at 60°C, then dialyzed the mixture with ddH_2O for 3 days to remove LiBr. Finally, we got the 5% (w/v) SF solution and stored it at 4°C.

2.3. Synthesis and characterization of Sr-SF-HA

Sr-SF-HA were synthesized by hydrothermal co-precipitation method using calcium chloride (CaCl2), strontium chloride (SrCl2), sodium phosphate (Na3PO4), and SF solution [19]. Firstly, 2.4975 g CaCl2 and 0.3963 g SrCl2 were dissolved in 40 mL deionized water, then 10 mL 5% (w/v) SF solution was added and evenly mixed, and then, dissolved 5.7 g Na_3PO_4 and 0.2 g NaOH in 50 mL ddH_2O and evenly mixed. Next, the solution containing Na_3PO_4 and NaOH was added drop by drop into the SF solution containing SrCl2 and CaCl2 to obtain the suspension and adjust the pH to 11. The suspension was stirred at 60°C for 24 h and aged at room temperature for 24 h. Then, the suspension was filtered to collect particles and washed with ddH_2O three times. Finally, dried the particles at 60°C for 48 h. The synthesis of SF-HA was similar to that of Sr-SF-HA, except that SrCl2 is not added.

The transmission electron microscope (TEM, JEM-2100, Japan) equipped with energy dispersive spectroscopy (EDS) was used to characterize the morphology and elemental composition of the Sr-SF-HA. X-ray diffraction (XRD, PANalytical X'Pert powder, Almelo, Netherlands) was used to assess the crystal phase and crystallinity of the particles. The surface elemental composition was assessed by X-ray photoelectron spectroscopy (XPS, Shimadzu Kratos AXIS Ultra DLD, Nagoya, Japan). And the surface functional groups were performed by Fourier transform infrared (FTIR, WQF-530, Beifen-Ruili, China) spectrum.

2.4. Preparation and characterization of CS/Sr-SF-HA

CS/Sr-SF-HA were prepared using the electrostatic spraying method. In short, 1 g CS powder and 0.25 g Sr-SF-HA were suspended in 40 mL ddH2O, and then 10 mL 5% (w/v) SF solution was stirred to form a uniform suspension. Next, 1% (v/v) acetic acid was added to form the final mixture. The mixture was then loaded into a plastic syringe. A collection tank containing a 5 wt% NaOH solution was placed 10 cm below the 21G nozzle. The nozzle and collector were respectively connected to 16 and -4 kV high-voltage power supply, and the injection speed was set to 0.1 mm/min. Then, the prepared microspheres were collected and washed with PBS three times and freeze-dried for 24 h. The preparation of CS/SF and CS/SF-HA was similar to that of CS/Sr-SF-HA. The morphology of microspheres was characterized by field emission scanning electron microscopy (Sigma 300, ZEISS, Germany). The samples were sputtered with gold, and then the structural images of the microspheres were collected.

2.5. Cell biocompatibility

rBMSCs and HUVECs were adopted to detect the cytotoxicity of the microspheres. rBMSCs were cultured in α-MEM containing 10% fetal bovine serum (FBS) and 1% penicillin/streptomycin in the incubator with 5% CO_2 at 37°C. The medium was changed every three days until the cells reached 80% confluence, and P3 cells were selected for subsequent experiments. HUVECs were cultured in high glucose DMEM containing 10% FBS and 1% penicillin/streptomycin in the incubator with 5% CO_2 at 37°C.

Microspheres were irradiated under ultraviolet light for 12 h to achieve sterility. After that, they were soaked in 75% alcohol for 30 min and then washed with sterilized PBS 3 times. Next, 35 mg/mL microspheres were soaked in the complete medium for 24 h to obtain extracts. For the CCK-8 test, cells (3×10^3 cells/well) were firstly seeded on 96-well plates, then the extracts were added into the corresponding wells. At 1, 4, and 7 days after inoculation, 10 μL CCK-8 solution was added to the 96-well plates, and the absorbance (OD) at 450 nm was measured with a microplate reader (TECAN Infinite M200PRO, China) after incubated for 1 h. For Live/Dead staining, cells (5×10^3 cells per well) were seeded on 24-well plates, and then the extracts were added to the corresponding wells. After co-culture for 1, 4, and 7 days, cells were incubated with live/dead staining solution and observed under a fluorescence microscope (DMI8, Leica, Germany).

2.6. In vitro osteogenesis capacity

For alkaline phosphatase (ALP) staining, rBMSCs were seeded in the 12-well plates at a density of 5×10^4 cells per well with complete medium and cultured to 80% confluence. Next, the complete medium was replaced by the extracts. After culturing for 4 and 7 days, 4% paraformaldehyde was added into the 12-well plates for 20 min to fix the rBMSCs. Next, cells were stained with BCIP/NBT alkaline phosphatase color development kit for 1 h at 37°C. For alizarin red staining (ARS), cells were cultured in the 12-well plates with the extracts as described above. After culturing for 14 and 21 days, the calcium depositions were stained by an ARS solution.

rBMSCs were inoculated in the 6-well plates and cultured until 90% confluence, and then, the complete culture medium was replaced with extracts. After 4 and 7 days of culture, a total RNA extraction kit was used to lyse rBMSCs and collect RNA. Next, the Revert Aid First Strand cDNA synthesis kit was used to obtain the cDNA. Then, the expression of three osteogenic-related genes, including alkaline phosphatase (*ALP*), runt-related transcription factor 2 (*RUNX2*), and osteopontin (*OPN*), was quantitatively measured by Real-time fluorescence quantitative PCR (qRT-PCR). All primers were obtained from Sangon Biotech Co., Ltd. (Shanghai, China). The qRT-PCR primer sequence is shown in Table 1.

Table 1
Primer sequences in the qRT-PCR studies.

Genes	Sequences
Rat GAPDH	F:5'-TTTGAGGGTGCAGCGAACTT-3'
	R:5'-ACAGCAACAGGGTGGTGGAC-3'
Rat ALP	F:5'-AACAACCTGACTGACCCTTCC-3'
	R:5'-CAATCCTGCCTCCTTCCAC-3'
Rat OPN	F:5'-GACGATGATGACGACGATGAC-3'
	R:5'-GTGTGCTGGCAGTGAAGGACTC-3'
Rat RUNX2	F:5'-TCCGCCACCACTCACTACCAC-3'
	R:5'-GGAACTGATAGGACGCTGACGAAG-3'

The expression of osteogenesis-related proteins in rBMSCs was further studied by western blotting and immunofluorescence. For western blotting, the total protein extraction of rBMSCs was processed using the protein extraction kit (KeyGen Biotech Co. Ltd). The proteins were migrated to polyvinylidene difluoride (PVDF) membranes and combined with specific antibodies to GAPDH (ab181602, Abcam), OPN (ab8448, Abcam), or RUNX2 (ab92336, Abcam). Then, goat anti-rabbit or anti-mouse antibodies were combined with the specific antibodies for 1 h. An Affinity ECL western blotting substrate was used to develop the immunoreactive bands and visualized by the ECL system. For immunofluorescence, rBMSCs (5×10^3 cells/well) were inoculated in a 12-well plate. On day 4, cells were fixed with 4% paraformaldehyde at 4°C for 30 min after washing with ddH_2O three times. Next, cells were treated with 0.5% Triton X-100 for 30 min and incubated with 5% goat serum for 1.5 h. Then, it was incubated with OPN and RUNX2 (1:100) overnight, respectively. Next, the cells were incubated with the secondary antibody (1:200) in the dark at room temperature for 1 h. The cytoskeleton was stained by F-actin (1:200) for 30 min, and the nucleus was stained by DAPI for 30 min. Finally, the expression of OPN and RUNX2 was detected by a fluorescence microscope (Bx53, Olympus, Japan), and the quantitative analysis of fluorescence intensity was analyzed with Image J.

2.7. In vitro angiogenesis capacity

After sterilization, microspheres were soaked in DMEM to obtain extracting solutions (35 mg/mL). For the tube formation test, the matrigel was added to the 96-well plates and then incubated at 37°C for 30 min. Subsequently, 3×10^4 HUVECs were suspended in different extracts and inoculated into the corresponding well. Then, cells were observed with a microscope (DMI8, Leica, Germany) after 10 h of culture.

For the cell migration experiment, the cells were seeded in the 6-well plates and cultured to reach 90% confluence. Then, 1 mL pipette tip was used to scrape off a straight line through the middle of the cells. The cells were cultured for 24 h with extracts after washing with PBS, and then the microscope was used to collect the pictures. The results were then analyzed with Image J.

For the qRT-PCR test, the cells were seeded on 6-well plates and cultured to reach 90% confluence, and then the complete medium was replaced by extracts for culture. After 1 and 3 days of cultivation, the expressions of the angiogenesis-related gene, such as vascular endothelial growth factor (*VEGF*) in HUVECs, were quantitatively measured by qRT-PCR in the same way as described above. The qRT-PCR primer

Table 2
Primer sequences in the qRT-PCR studies.

Genes	Sequences
Human GAPDH	F:5'-GTCTCCTCTGACTTCAACAGCG-3'
	R:5'-ACCACCCTGTTGCTGTAGCCAA-3'
Human VEGF	F:5'-CACGACAGAAGGAGAGCAGAAGTC-3'
	R:5'-GTCTCAATCGGACGGCAGTAGC-3'

sequence is shown in Table 2.

The expression of angiogenesis-related proteins in HUVECs was further studied by immunofluorescence, and VEGF was detected by fluorescence microscope. The specific operation is consistent with the above description.

2.8. *In vivo osteogenesis and angiogenesis ability*

All animal experiments were approved by the Ethics Committee of Southwest Medical University with approval number 20221212-006 and

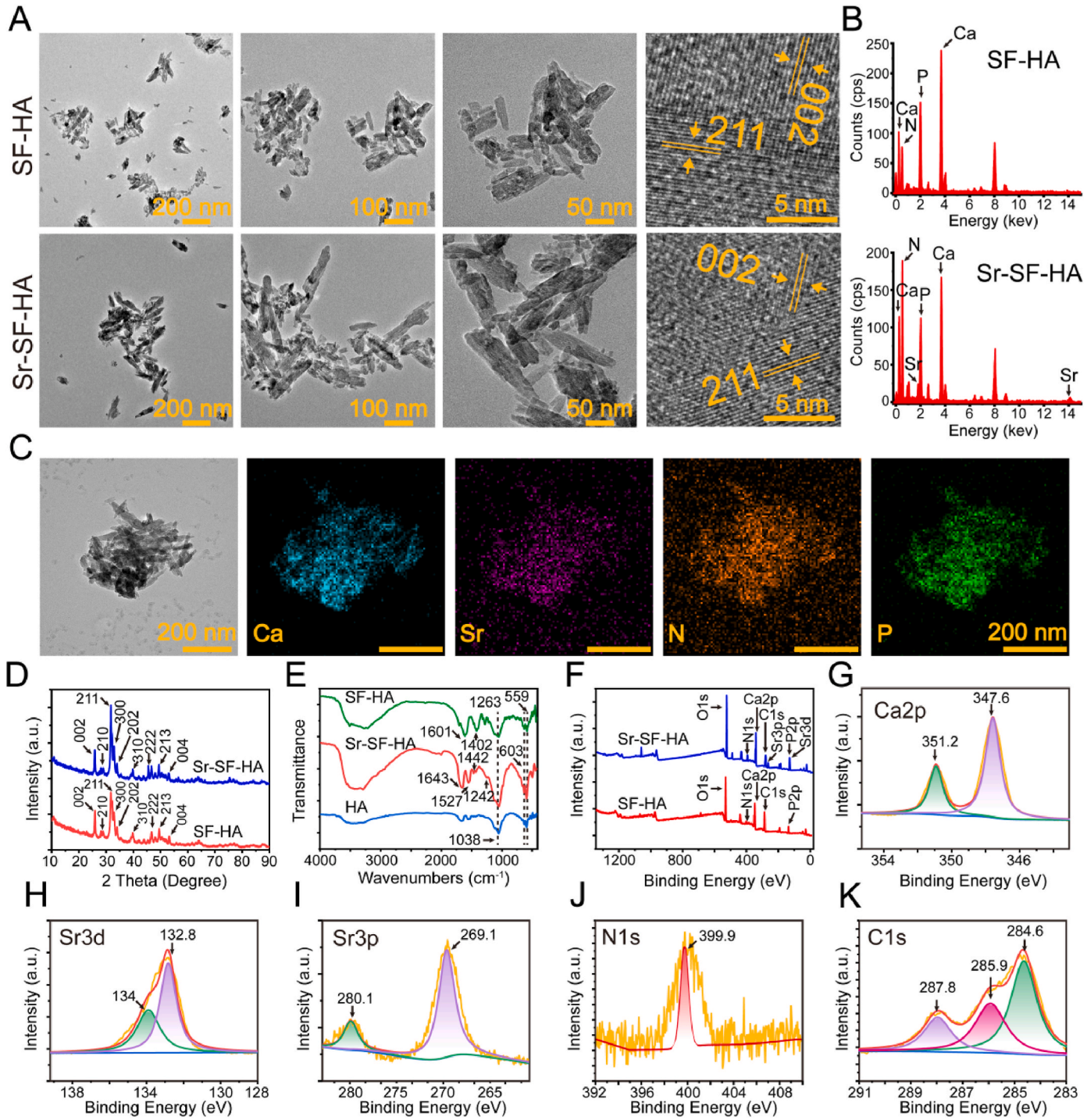

Fig. 2. Characterization of synthesized SF-HA and Sr-SF-HA. (A) TEM images of SF-HA and Sr-SF-HA. (B) EDS detection of SF-HA and Sr-SF-HA. (C) EDS mapping of Sr-SF-HA. (D) XRD spectra and (E) FTIR spectra of SF-HA and Sr-SF-HA. (F) XPS spectra of SF-HA and Sr-SF-HA. (G–K) High-resolution spectra of Ca 2p, Sr 3d, Sr 3p, N 1s, and C 1s, respectively.

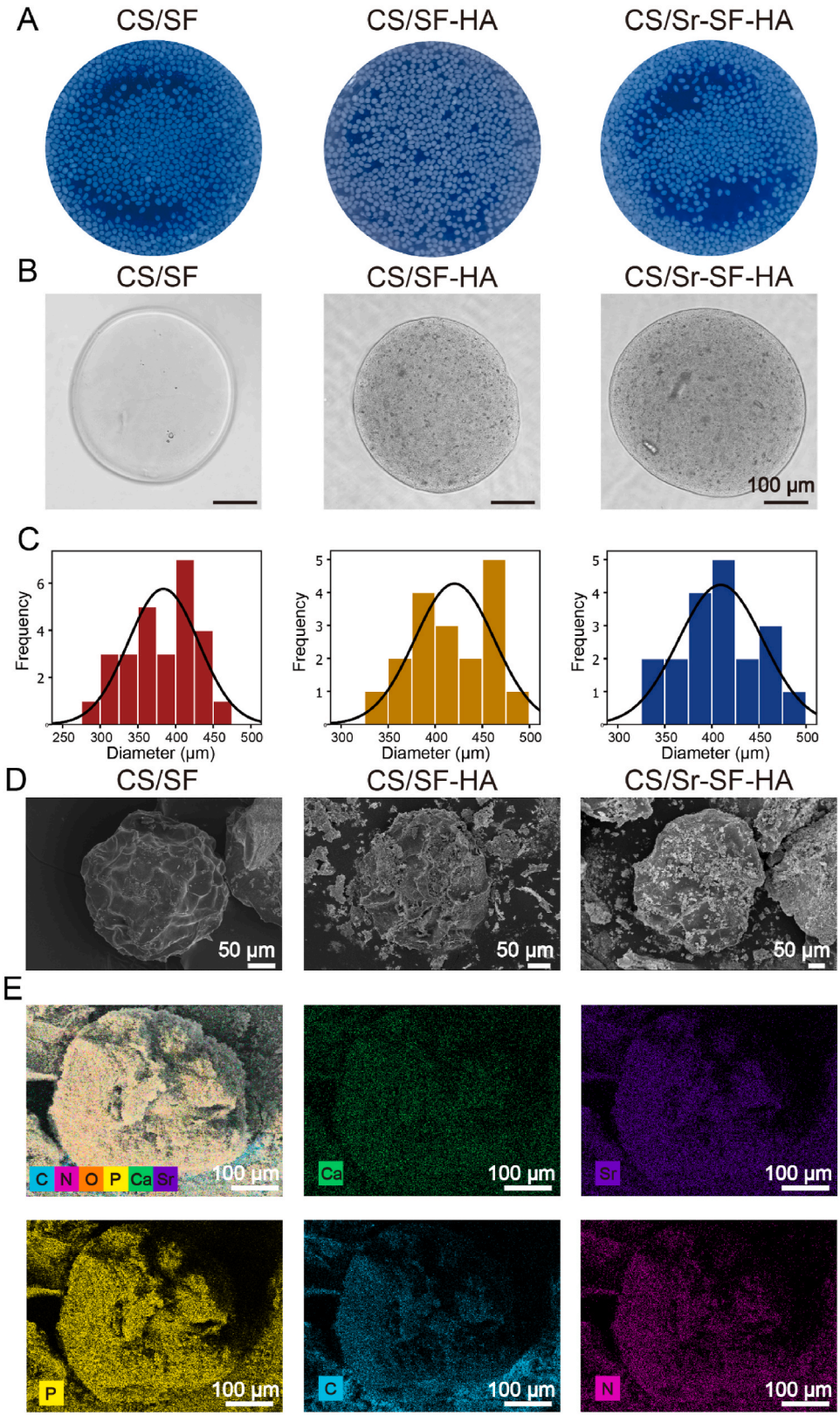

Fig. 3. Characterization of prepared microspheres. (A) Pictures of three groups of microspheres. (B) Photomicrograph of microspheres. (C) Particle size analysis of microspheres. (D) SEM of microspheres. (E) EDS mapping of CS/Sr-SF-HA microsphere.

performed under the guidance of the Animal Care Committee. Sprague-Dawley male rats (8 weeks old, weighing 300 g, Experimental Animal Center of Southwest Medical University) were anesthetized by inhalation of isoflurane. After shaving the back hair, a scalpel was used to make three 1 cm long incisions on the back, and used a vascular clamp to separate the skin to form three subcutaneous pockets, then implanted 10 mg sterilized microspheres into the corresponding subcutaneous pockets respectively and sutured the incision.

The animals were euthanized after 2, 4, and 8 weeks, and tissues were collected and fixed with 4% paraformaldehyde, then dehydrated and embedded in paraffin. Histological, immunofluorescence, and immunohistochemical experiments were performed with sections within 5 μm thickness. Hematoxylin-eosin (HE) and Masson's trichrome staining were carried out on consecutive tissue sections. Then, images were obtained with digital slice scanning equipment (KF-PRO-002, China). For immunofluorescence, CD31 antibody (Servicebio) was used to incubate the sections at 4°C for 24 h, and then Cy3 goat anti-rabbit IgG was applied to incubate the sections at room temperature for 2 h. And DAPI was used to stain the nuclei. Then, sections were observed using a fluorescence microscope. In addition, the immunohistochemical analysis was used to analyze the expression of COL-1 and OCN in tissues. The paraffin slices were dewaxed. Next, the sections were incubated overnight with primary antibodies against type I collagen (Col-I) and osteocalcin (OCN) in a closed solution at 4°C at a dilution of 1:200 after repairing the antigen with sodium citrate. Then, after washing the slices with PBS, the samples were combined with rabbit anti-goat IgG second antibody (Alexa Fluor 647, Invitrogen) at a dilution of 1:100 and incubated at room temperature in darkness for 1 h. Finally, the slices were restained with hematoxylin, and images were captured with digital slide scanning equipment.

2.9. Statistical analysis

All results were expressed as mean ± standard deviation (SD). One-way analysis of variance (ANOVA) was performed, and then the Tukey multiple comparison test (GraphPad Prism 8, USA) was performed. The p value < 0.05 was accepted as statistical significance (*$p < 0.05$, **$p < 0.01$, ***$p < 0.001$, ****$p < 0.0001$).

3. Results and discussion

3.1. Synthesis and characterization of Sr-SF-HA nanoparticles

Hydroxyapatite (HAp) and its ion-substituted derivatives are promising materials for bone tissue engineering. Previous studies have shown that HAp can be endowed with biological functions such as osteogenesis, angiogenesis, and immunomodulation by ion substitution [13,14]. Inspired by the biomineralization process, hydroxyapatite has been synthesized by a biomimetic mineralization strategy using natural proteins, including collagen and gelatin. Silk fibroin is a natural protein secreted by the silkworm, which initiates and directs the growth of bone apatite through a biomimetic synthesis [28,39,40].

In this study, sr-substituted hydroxyapatite was self-assembled with a silk fibroin template. Firstly, TEM analysis was carried out to characterize the morphology of the particles. It could be found that SF-HA and Sr-SF-HA were both nano-rod structures. In addition, the characteristic lattice spacing of HAp could be observed in high magnification images, including d-spacings of 0.334 nm corresponding to the distance of the (002) plane and 0.272 nm corresponding to the distance of the (211) plane of HAp, respectively [41] (Fig. 2A). Through EDS detection, it could be found that the Ca/P ratio in SF-HA was 1.57 and the (Ca + Sr)/P ratio in Sr-SF-HA is 1.56. The results were both close to 1.67, which was nearly the Ca/P ratio of natural hydroxyapatite [42] (Fig. 2B). In addition, it could be found that the Ca, Sr, and P elements in Sr-SF-HA nanoparticles were uniformly distributed, indicating that Sr was uniformly doped in Sr-SF-HA after partially replacing Ca (Fig. 2C). And the uniform distribution of N elements indicating the presence of silk fibroin. X-ray diffraction (XRD) results showed that both SF-HA and Sr-SF-HA with characteristic diffraction peaks of HAp crystal (JCPDS no. 09–0432) at (002), (210), (211), (300), (202), (310), (222), and (213) without any displacement or new peak. These results implied that adding strontium did not influence the crystal phase of HAp (Fig. 2D).

The results of the FTIR spectra showed the presence of absorption spectra of three characteristic amide bands in SF-HA and Sr-SF-HA, namely the peaks of amide I range from 1600 to 1700 cm^{-1}, amide II range from 1540 to 1530 cm^{-1}, and amide III range from 1400 to 1500 cm^{-1} and 1200-1400 cm^{-1}, which confirmed the presence of SF [23,43]. In addition, the antisymmetric stretching of $\nu 3$ P–O was considered to cause the strong spectral band at 1038 cm^{-1}, while the bending vibration of $\nu 4$ P–O was considered to cause the absorption bands at 603 cm^{-1} and 559 cm^{-1}, respectively [17,44–46]. Clearly, the distinct peak (1038 cm^{-1}, 603 cm^{-1}, and 563 cm^{-1}) detected in the particles was the PO_4^{3-} group, which further proved the successful synthesis of HAp (Fig. 2E).

Furthermore, the chemical composition and chemical state of SF-HA and Sr-SF-HA were observed by XPS. Through full XPS spectroscopy, it can be observed that Sr-SF-HA contained elements Sr, Ca, N, P, O, and C, while SF-HA contained elements Ca, N, P, O, and C (Fig. 2F). The detailed information on the chemical composition of Sr-SF-HA could be detected by studying the peaks fitting results of Ca 2p, P 2p, Sr 3d, N 1s, and C 1s. The peak of Ca 2p (Ca 2p3/2 at 347.6 eV/Ca 2p1/2 at 351.2 eV) corresponds to the Ca^{2+} (Fig. 2G), whereas the P2p peak at 132.7 eV was assigned to $PO4^{3-}$. Sr 3p and Sr 3d are two major peaks of strontium. They were detected at 269.1 eV (Sr 3p3/2), 280.1 eV (Sr 3p1/2), 134 eV (Sr 3d3/2), and 132.8 eV (Sr 3d5/2) (Fig. 2H and I). Sr 3d and P 2p peaks overlapped because of their close binding energies in the spectrum [46,47]. These results indicated the successful doping of Sr^{2+}. In addition, the peak of N 1s was detected at 399.9 eV, which was assigned to the secondary amine functionalities (-NH-) (Fig. 2J). The peak of C 1s (Fig. 2K) could be fitted at 284.6 eV, 285.9 eV, and 287.8 eV, corresponding to the three main components, including chemical bonds of C–C, C–O/C–N, and C═O/C═N, respectively [48]. The existence of C–N, -NH-, and C═O showed the presence of SF. In conclusion, the results of TEM, EDS, XRD, FTIR, and XPS indicated that the Sr-SF-HA and SF-HA nanoparticles were successfully synthesized using SF as the template.

3.2. Fabrication and characterization of CS/Sr-SF-HA microspheres

As a carrier, microspheres can be applied to irregular and complex shape bone defects while providing a high specific surface area to facilitate the release of functional substances. Microspheres effectively avoid the disadvantage of directly implanting nanoparticles [31]. Compared with emulsion and microfluidic technology, electrostatic spraying can better meet the needs of microspheres for *in vivo* applications such as controllable particle size distribution, quick and stable output, as well as low cost [49]. Thus, in our study, CS/Sr-SF-HA loaded with Sr-SF-HA were prepared by electrostatic spraying technique.

As shown in Fig. 3A, it could be observed that CS/SF, CS/SF-HA, and CS/Sr-SF-HA were all uniform and micrometer-sized. Specifically, through statistical analysis, the diameter of CS/SF, CS/SF-HA, and CS/Sr-SF-HA were 383.9 ± 76 μm, 420.5 ± 62 μm, and 409.4 ± 84.5 μm, respectively (Fig. 3C). And the SF-HA and Sr-SF-HA were uniformly distributed in the CS/SF-HA and CS/Sr-SF-HA (Fig. 3B). After freeze-drying, the microspheres were characterized by SEM. As shown in Fig. 3D, the three groups of microspheres were in quasi-spherical shape with grooved surfaces, suggesting that the freeze-dried microspheres had higher specific surface area to release substances more effectively. Besides, the uniform distribution of nanoparticles could be clearly observed on the surface of CS/SF-HA and CS/Sr-SF-HA after incorporating 0.5% SF-HA and 0.5% Sr-SF-HA. Furthermore, through EDS detection, it could be observed that Ca, Sr, P, C, and N elements were uniformly distributed on CS/Sr-SF-HA, indicating that the nanoparticles on the surface of CS/Sr-SF-HA were Sr-SF-HA (Fig. 3E). In conclusion, these results confirmed the successful preparation of CS/SF, CS/SF-HA, and CS/Sr-SF-HA, laying the foundation for the subsequent function test.

3.3. Cytotoxicity and biocompatibility of microspheres

Excellent biocompatibility is necessary for the application of composite microspheres in the repair of bone tissue defects [50–52]. The

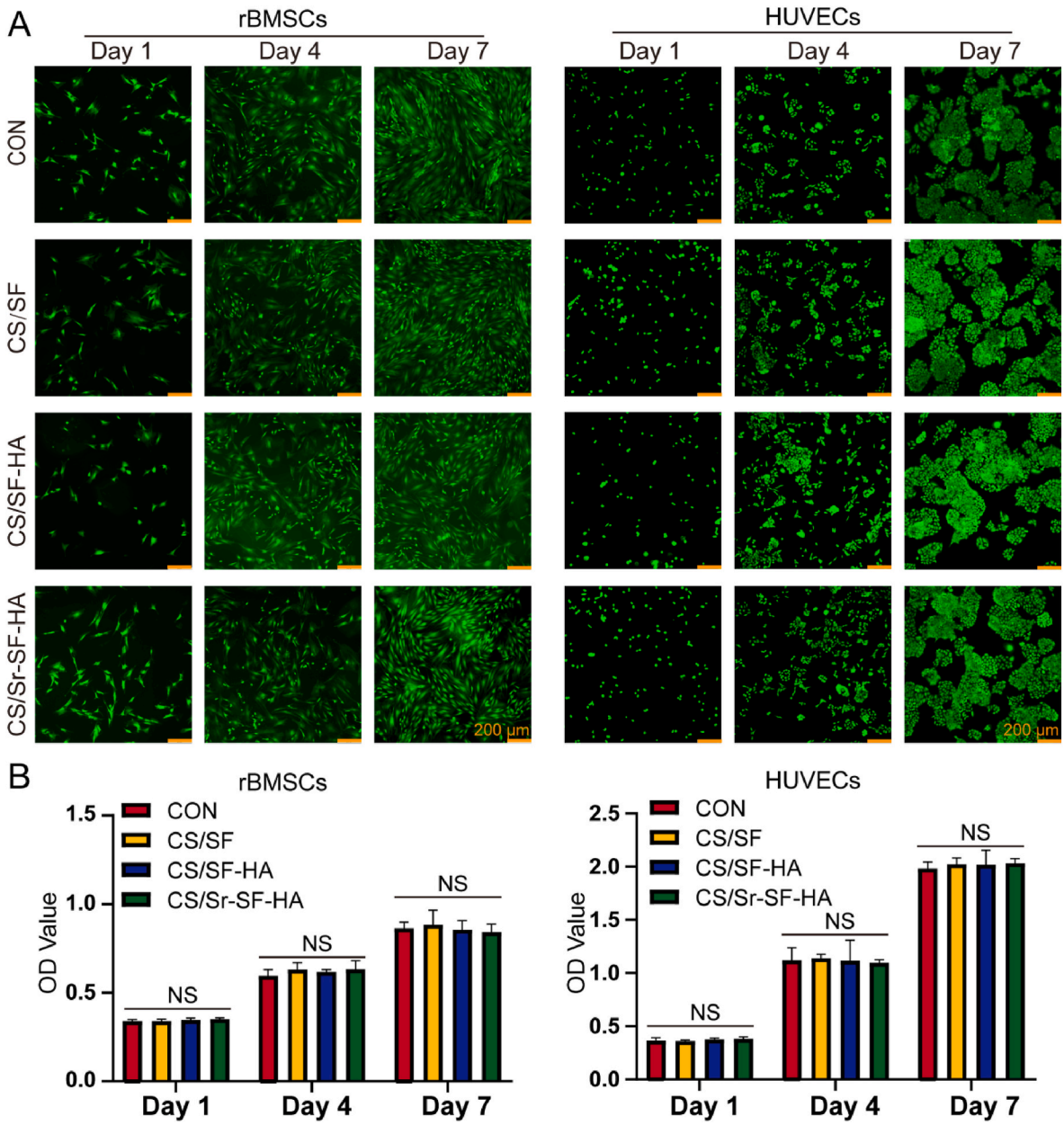

Fig. 4. Cytotoxicity and cell proliferation of microspheres. (A) Live/dead staining. (B) CCK-8 assay at 1, 4, and 7 days.

cytocompatibility of biomaterial scaffolds can be accurately detected by co-culturing extracts of biomaterial scaffolds with cells [53]. Here, extracts of CS, CS/SF-HA, and CS/Sr-SF-HA were co-cultured with rBMSCs and HUVECs respectively, and subjected to live/dead staining and CCK-8 analysis on days 1, 4, and 7. As the culture time increased, the cells in the experimental groups all had good growth status, and the number of live cells grew apparently. Meanwhile, there was no significant difference between each microsphere treatment group and the control group (Fig. 4A).

We further performed CCK-8 assays to detect the effect of microspheres on cell proliferation. The cell viability of rBMSCs and HUVECs co-cultured with CS, CS/SF-HA, and CS/Sr-SF-HA increased with time at days 1, 4, and 7, and there was no significant difference between the microsphere-treated groups and control group (Fig. 4B). Thus, the results of CCK-8 assay and live/dead staining showed that the microspheres had good biocompatibility and did not affect the cell viability of rBMSCs and HUVECs.

3.4. *In vitro angiogenesis*

In the process of bone remodeling and repair, the vascular network play an important role in secreting cytokines, recruiting cells, and transporting oxygen and nutrients [12,54]. Therefore, angiogenesis is a key component in achieving functional bone regeneration and repair. Cell migration is of great significance in the process of angiogenesis [32]. Here, the scratch wound healing assays were performed to test the influence of different microsphere extracts on the migration behavior of HUVECs. As shown in Fig. 5A and C, after treating the scratched wounds with the microsphere extracts for 24 h, HUVECs in the CS/Sr-SF-HA treated group migrated at a higher rate than the remaining three groups. Strontium ions have been shown to have the ability to accelerate cell migration [15]. In our study, strontium ions released from CS/Sr-SF-HA microspheres stimulated HUVECs migration, which may provide further evidence for promoting angiogenesis.

Matrigel tube formation assay for further assessment of the contribution of CS/Sr-SF-HA to the angiogenic capacity of HUVECs. As shown

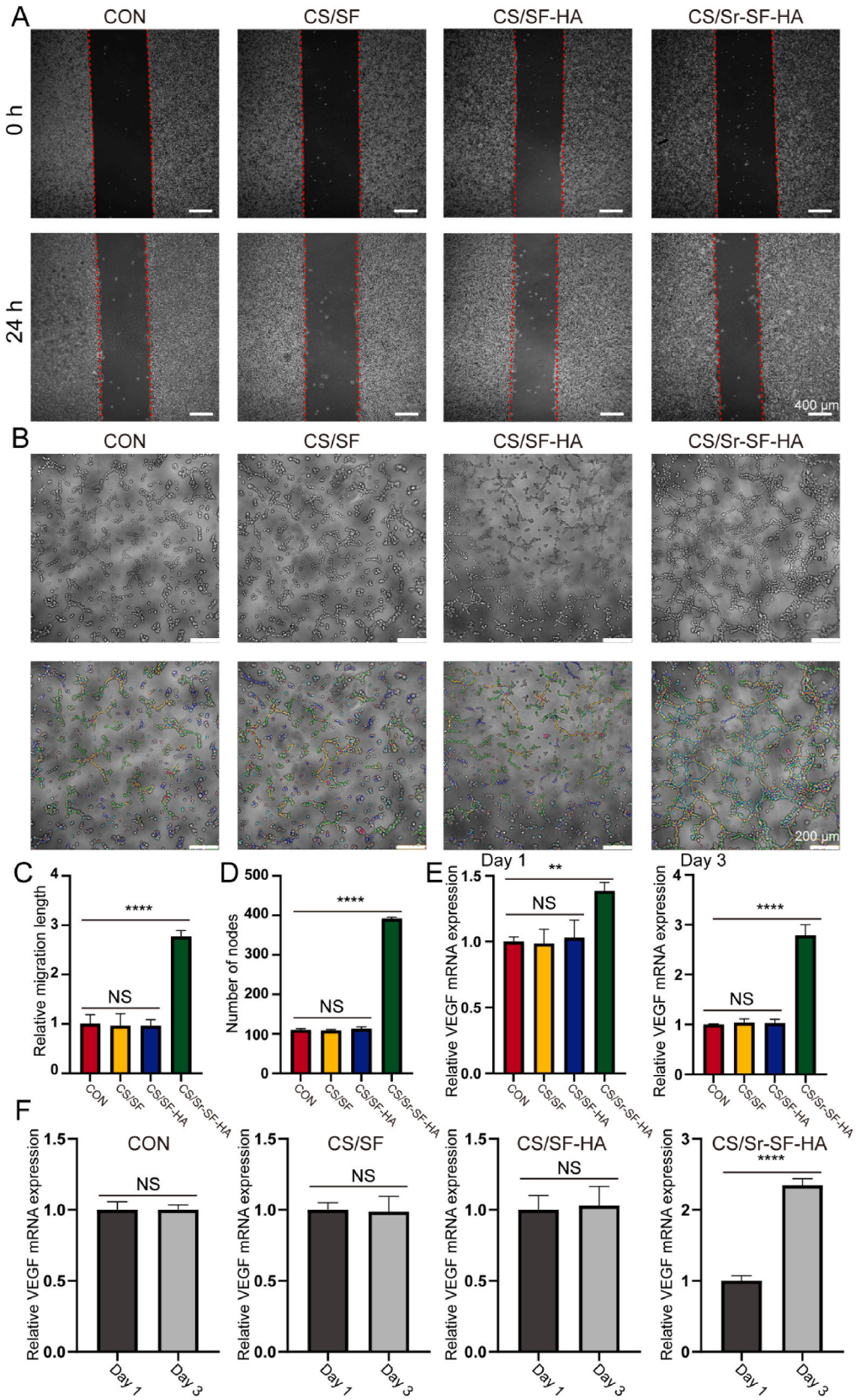

Fig. 5. *In vitro* angiogenesis potential of microspheres. (A) Scratch test at 24 h and (C) quantitative analysis. (B) Tube forming experiment of 10 h and (D) quantitative analysis. (E) Angiogenesis-related gene expression analysis on day 1 and day 3. (F) Angiogenesis-related gene expression analysis in the same group on day 1 and day 3.

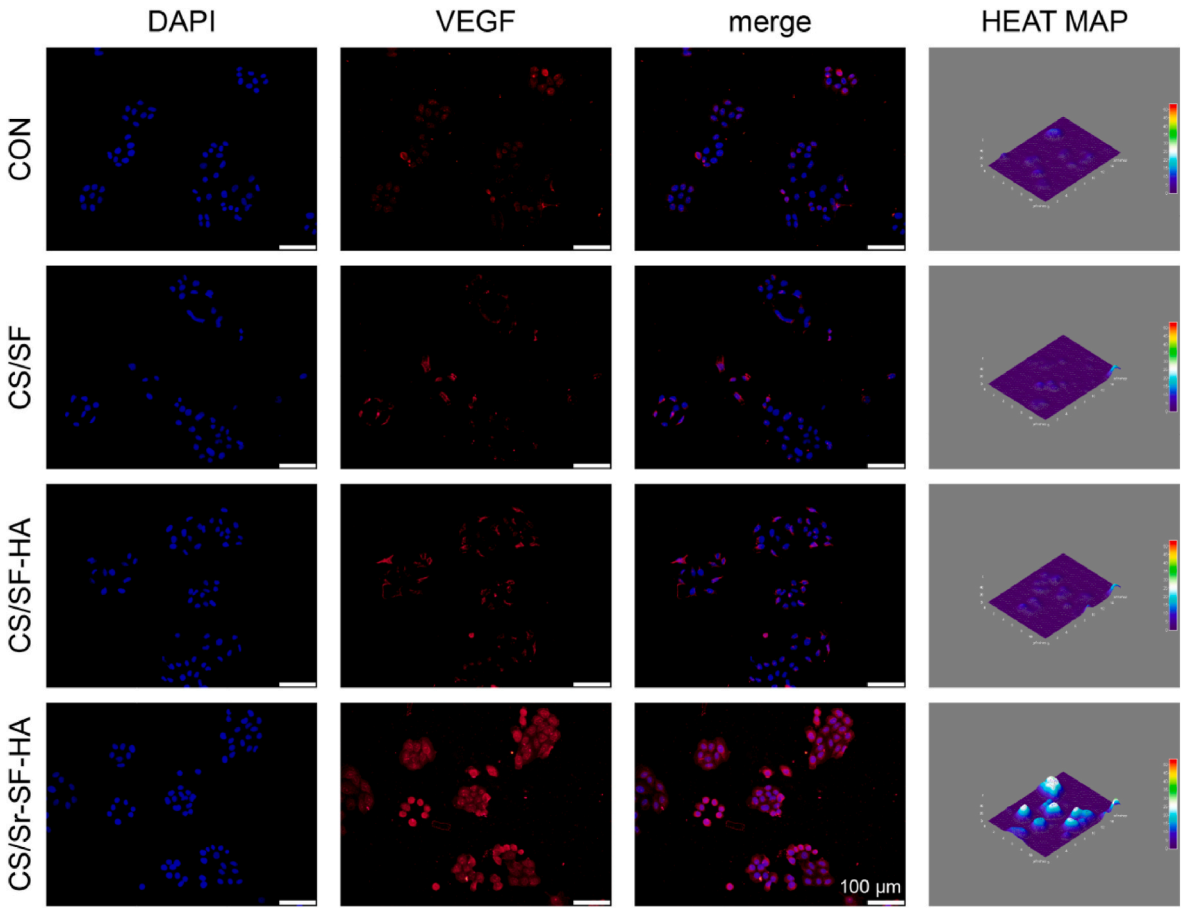

Fig. 6. VEGF immunofluorescence staining of HUVECs on day 3.

in Fig. 5B, HUVECs in the group treated with CS/Sr-SF-HA had significantly more vascular tube formation, whereas the CON, CS/SF, and CS/SF-HA treated group formed very few incomplete tubular structures. The number of nodes was apparently higher in the CS/Sr-SF-HA treated group, which further demonstrated that CS/Sr-SF-HA could enhance angiogenesis *in vitro* (Fig. 5D).

VEGF is a highly specific vascular endothelial growth factor that can enhance the migration and proliferation ability of vascular endothelial cells, improve vascular permeability, and promote angiogenesis [8,55,56]. Wu X et al. found that strontium ion promotes endothelial cell migration and vascularization by up-regulating the VEGF-mediated signaling pathway [57]. In this study, the results of qRT-PCR showed that compared with the other three groups, the CS/Sr-SF-HA treatment group could significantly increase the expression of VEGF at days 1 and 3 (Fig. 5E). As shown in Fig. 5F, with the increase of culture time, the expression of VEGF in CON, CS/SF, and CS/SF-HA groups did not show significant changes, while the expression of VEGF in CS/Sr-SF-HA group showed a significant increase compared to the first day, indicating that the presence of Sr ions could consistently affect the angiogenic capacity of HUVECs. Furthermore, we detected the protein expression of VEGF by immunofluorescence staining. Through fluorescence semi-quantitative volcanic map, it could be observed that the expression of VEGF in the CS/Sr-SF-HA group was significantly higher than the control group, CS/SF, and CS/SF-HA group (Fig. 6). The above findings suggested that the CS/Sr-SF-HA could promote HUVECs migration and rapid vessel formation *in vitro*.

3.5. *In vitro osteogenesis*

Alkaline phosphatase (ALP), a marker of early osteogenesis, is mainly distributed in the binding transport proteins of the cell membrane and promotes the maturation and calcification of osteoblasts [58]. The expression of ALP reflects the differentiation of osteoblasts, with higher activity indicating more pronounced pre-osteoblastic differentiation [59]. Therefore, we used ALP staining to assess the influence of CS/Sr-SF-HA as early markers of osteogenic differentiation in rBMSCs. As shown in Fig. 7A, the CS/Sr-SF-HA treated group showed better ALP activity than the CS/SF-HA group, while the blank control and CS/SF treated groups showed similar and weakest ALP expression activity. ALP expression activity increased from day 4 to day 7, and the trend was consistent.

Mineralized nodules are a sign of osteoblast differentiation and maturation; therefore, observation of mineralized nodules in osteoblasts is one of the common techniques for studying osteoblast differentiation [60]. Alizarin red (ARS) is a common staining method to observe mineralized nodules. In our study, ARS staining was performed on rBMSCs at day 14 and day 21 of culture with different microsphere extracts. As shown in Fig. 7B, the control and CS/SF groups of BMSCs produced a close and low number of calcareous nodules, whereas the CS/SF-HA group had more calcareous nodules and the CS/Sr-SF-HA group had the most calcareous nodules.

To further detect the mechanism of CS/Sr-SF-HA enhancing osteogenesis capacity, we analyzed the expression of osteogenesis-related genes of rBMSCs in different microsphere-treated groups by qRT-PCR. As shown in Fig. 7C, the expression of *ALP*, *OPN,* and *Runx2* in the CS/SF-HA group were significantly increased on the 4th and 7th day, and the expression of CS/Sr-SF-HA group was stronger than that in the CS/SF-HA group. The results showed that CS/Sr-SF-HA significantly enhances the expression of osteogenic-related genes and transcription factors. In short, the results of ALP, ARS, and qRT-PCR showed that pure

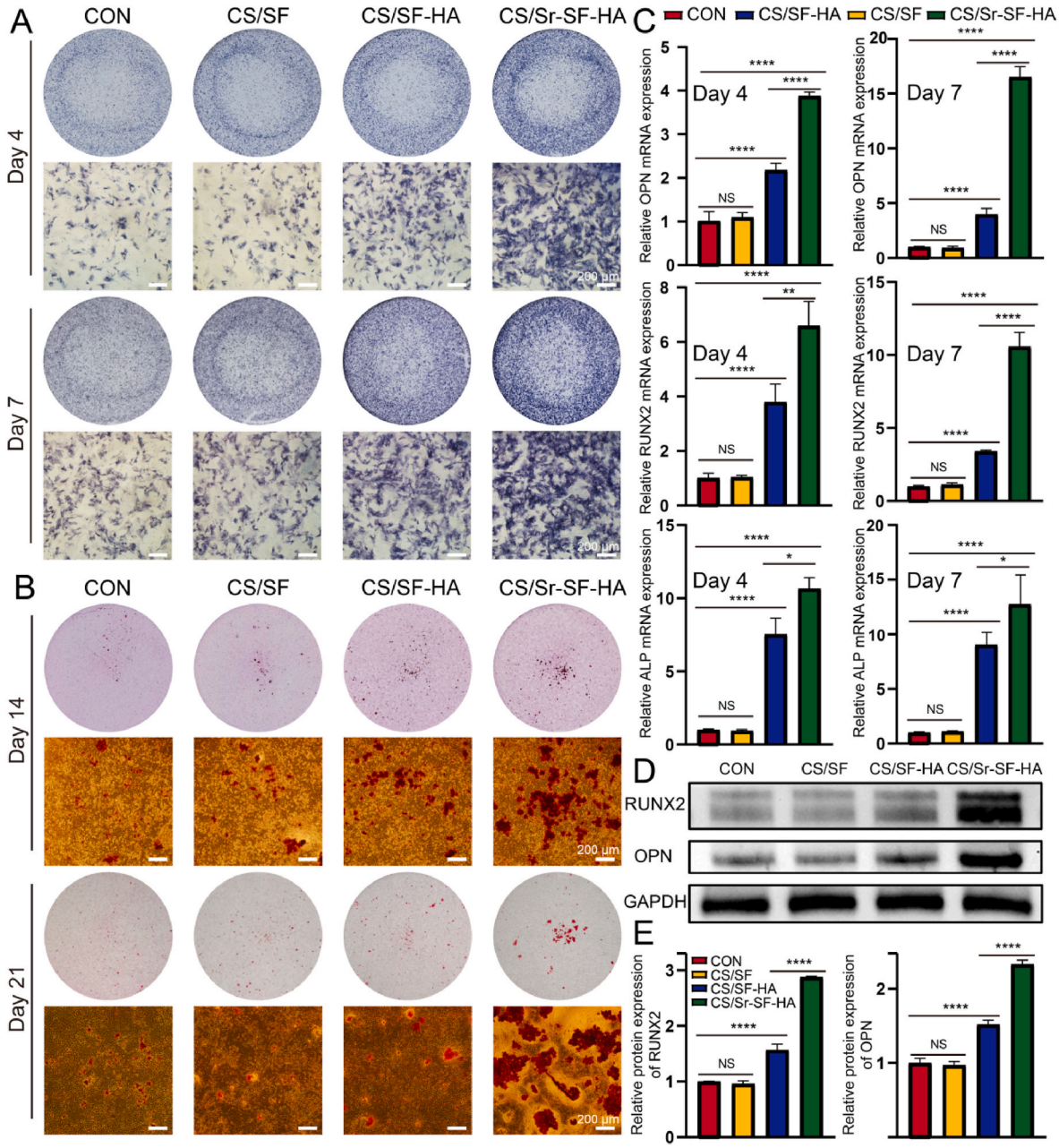

Fig. 7. *In vitro* osteogenesis potential of CS/Sr-SF-HA. (A) ALP staining on day 4 and day 7. (B) ARS on day 14 and day 21. (C) Osteogenic genes expression analysis on day 4 and day 7. (D) Osteogenic proteins expression analysis and (E) quantitative analysis on day 7.

CS/SF had no effect on the osteogenic ability of rBMSCs. Moreover, CS/Sr-SF-HA loaded with Sr-SF-HA promoted osteogenic differentiation of rBMSCs more effectively than CS/SF-HA, which might be due to the Sr ions released to enhance the early osteogenic differentiation potential of endogenous MSCs and thus produced a series of chain reactions [14,61].

Furthermore, we detected the protein expression of RUNX2 and OPN by immunofluorescence staining and western blotting to further elucidate the osteogenic performance and mechanism of the microspheres. RUNX2 is mainly expressed in osteoblasts derived from MSCs and is an important transcription factor determining the differentiation of MSCs into osteoblasts [62]. OPN is an essential extracellular non-collagenous matrix protein in bone tissue. It is highly expressed in mature osteoblasts and osteoclasts and is a characteristic marker of osteoblasts at the matrix formation and maturation stage, closely associated with bone formation and development [8,58]. The western blotting results showed that the expression of RUNX2 and OPN proteins in the CS/Sr-SF-HA group was significantly higher than in the CS/Sr-HA group. The expression of RUNX2 and OPN in the CS/SF group was similar to that in the control group, suggesting that they did not promote osteogenic capacity (Fig. 7D and E). The immunofluorescence staining results showed that on the 4th day after being cultured with the different microsphere extracts, all cells had good morphology and the expression of OPN in the cytoplasm and RUNX2 in the nucleus. Through fluorescence semi-quantitative volcanic map, it could be observed that the expression levels of OPN and RUNX2 in the CS/SF-HA group were significantly higher than the control group and CS/SF group. Moreover, the CS/SF-Sr-HA group had the highest expression level of OPN and RUNX2 protein (Fig. 8A and B). These results further indicated that CS/SF-Sr-HA can effectively promote the osteogenic differentiation of rBMSCs. Combined with various results, we could speculate that under the influence of CS/SF-Sr-HA, rBMSCs differentiated into osteoblasts under the control of RUNX2 and further synthesized extracellular matrix, including OPN. Then, cells released

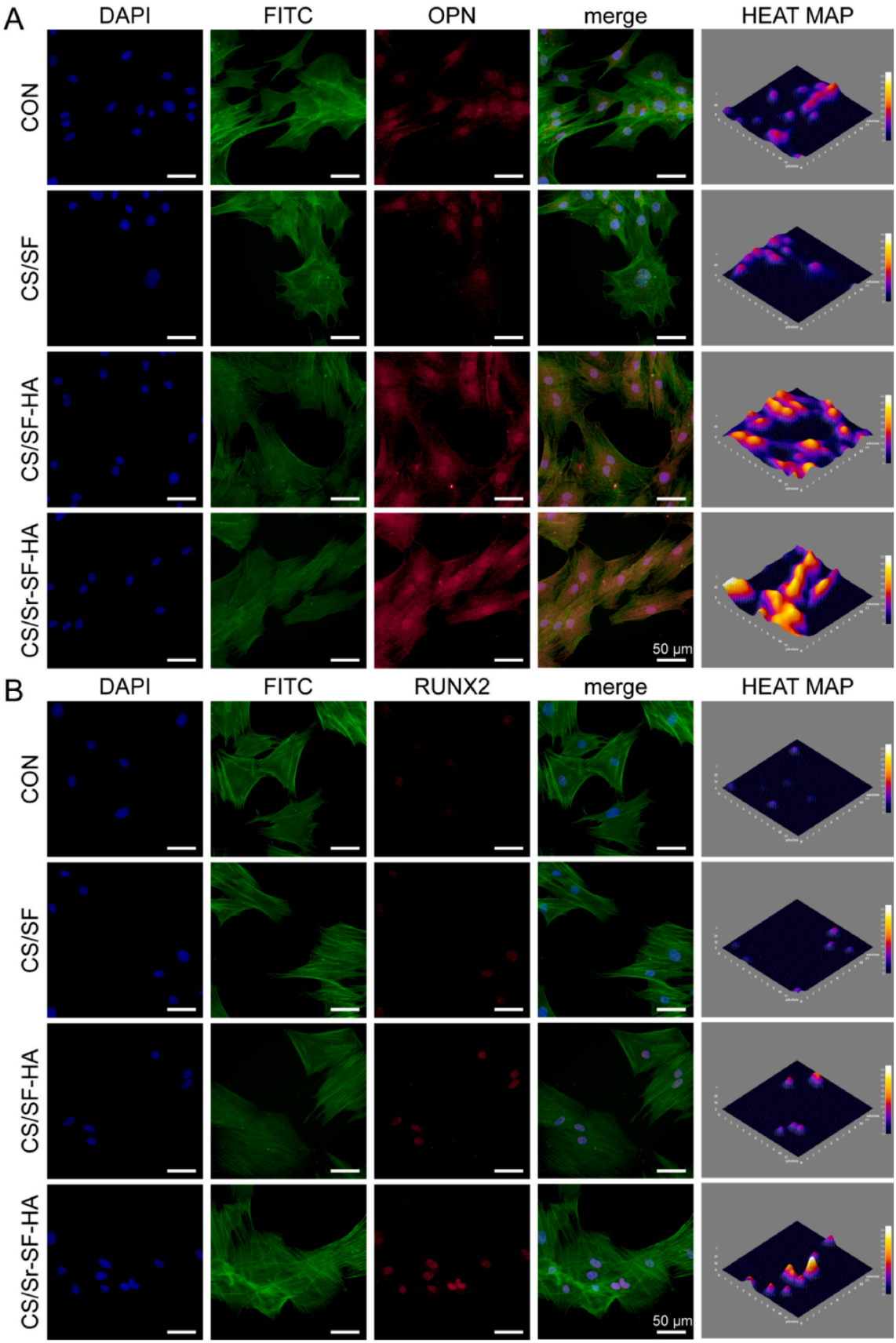

Fig. 8. (A) OPN and (B) RUNX2 immunofluorescence staining of rBMSCs on day 4.

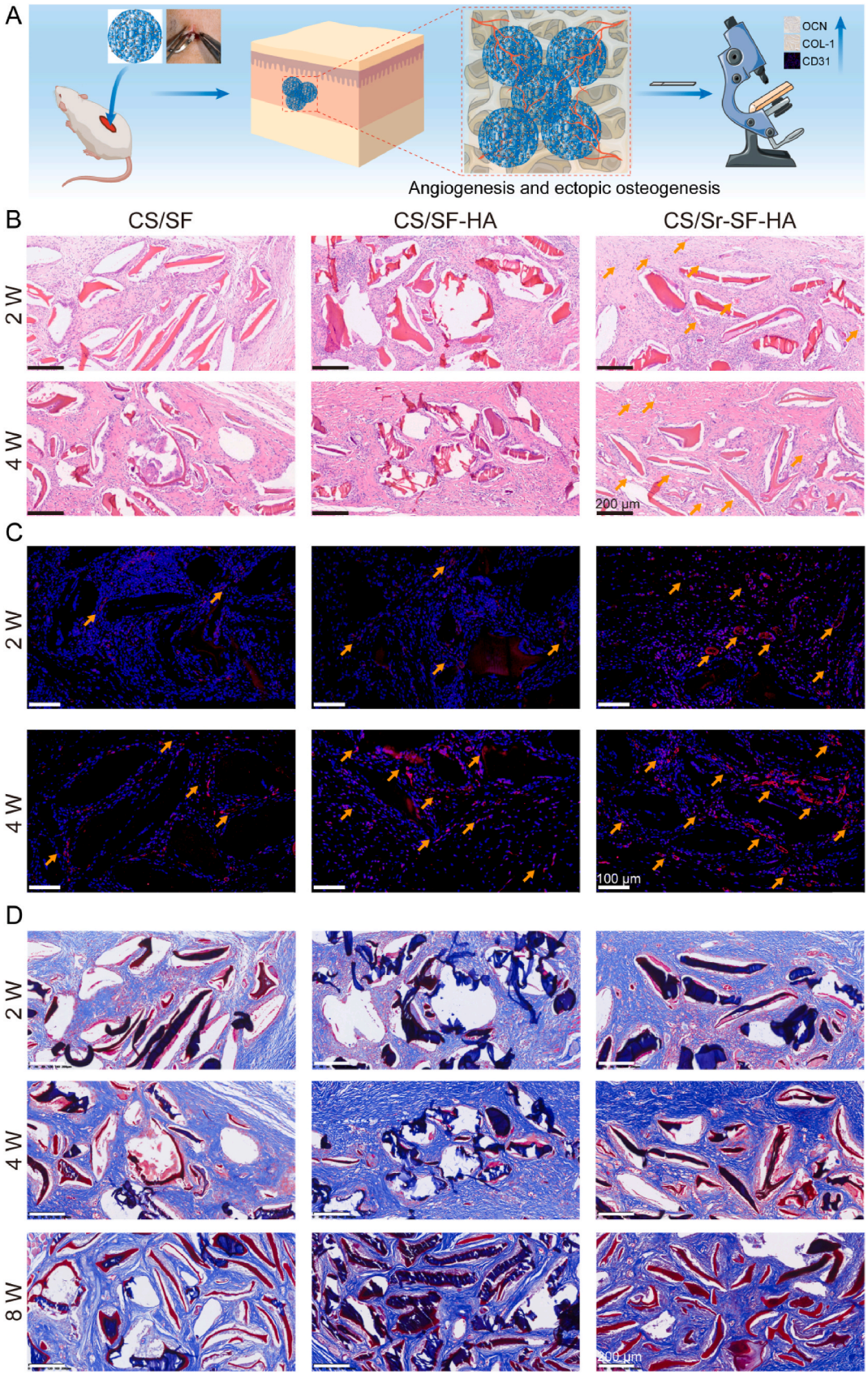

Fig. 9. *In vivo* subcutaneous angiogenesis and osteogenesis. (A) Schematic diagram of subcutaneous experiment. (B) HE staining at 2 and 4 weeks and (C) corresponding CD31 immunofluorescence staining images of different groups at 2 and 4 weeks. (D) Masson staining at 2, 4, and 8 weeks.

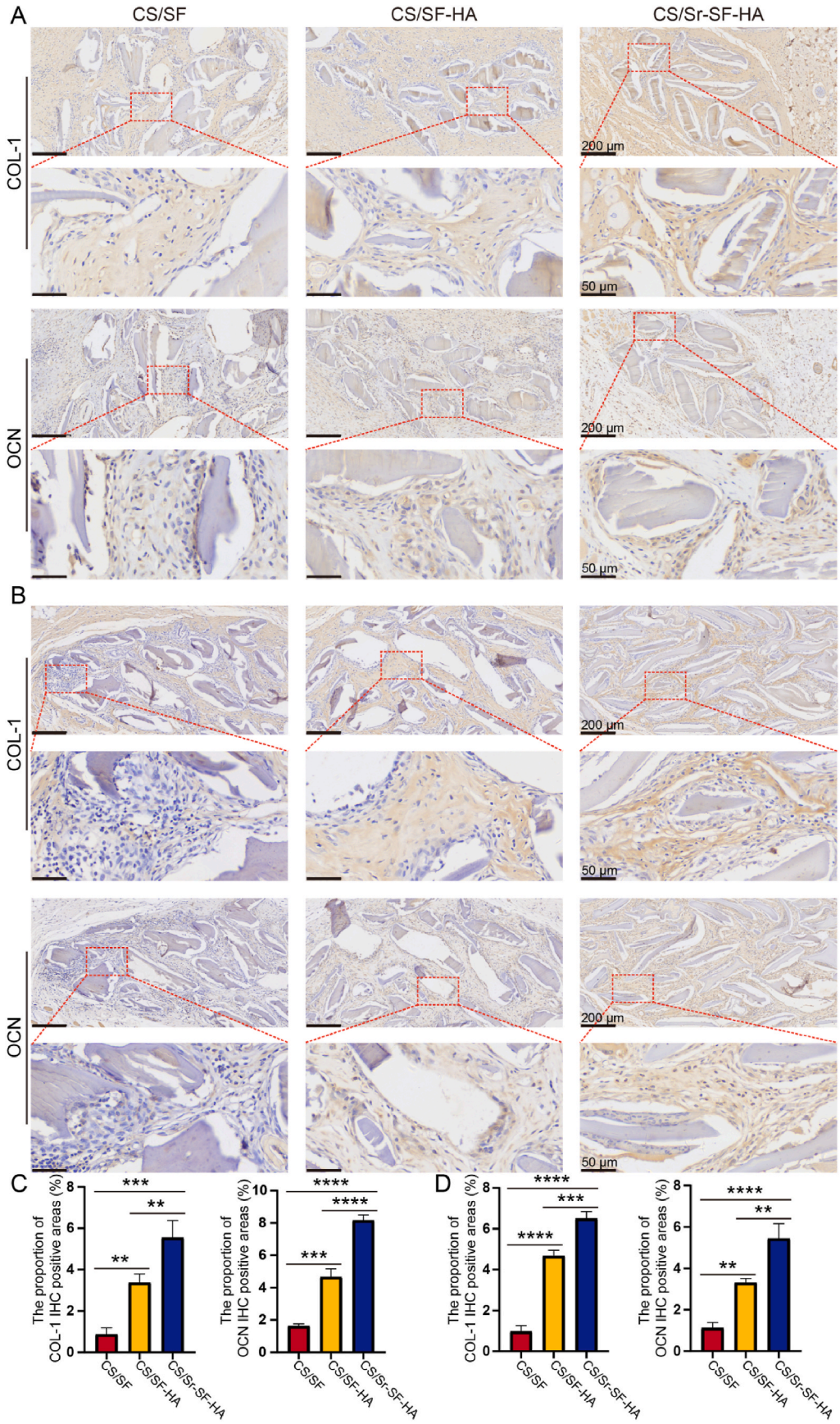

Fig. 10. *In vivo* ectopic osteogenesis. (A) Immunohistochemical results of COL-1 and OCN of microspheres treatment after 4 and (B) 8 weeks. Quantitative analysis of COL-1 and OCN immunohistochemical results at (C) 4 and (D) 8 weeks.

matrix vesicles containing calcium ions, alkaline phosphatase (ALP), and other enzymes. Next, under the action of ALP, Calcium ions deposed on the collagen filaments and finished the matrix mineralization process.

3.6. Evaluation of subcutaneous angiogenesis and osteogenesis with microspheres implantation

The microspheres (CS/SF, CS/SF-HA, and CS/SF-Sr-HA) were implanted into the back of rats for 2 months, and HE, Masson, immunofluorescence staining, and immunohistochemical staining were carried out to detect biocompatibility, promote angiogenesis and ectopic osteogenesis potential (Fig. 9A) [63,64]. After 2 and 4 weeks of treatment, the HE staining showed tight tissue growth around the microspheres, no tissue necrosis or infection was observed, and no significant inflammatory cell infiltration was detected, indicating that all the composite microspheres have excellent biocompatibility. Promisingly, neovascularization was clearly observed around the CS/Sr-SF-HA implantation site, whereas little neovascularization was observed at the CS/SF and CS/SF-HA implantation sites, either at week 2 or week 4 (as indicated by the arrows) (Fig. 9B).

CD31, a platelet-endothelial cell adhesion molecule, is usually located in vascular endothelial cells and participates in angiogenesis [56,65]. Higher CD31 expression means higher angiogenic activity and more blood vessels. The effect of the CS/Sr-SF-HA on angiogenesis was further examined by CD31 immunofluorescence staining of the tissue surrounding the microspheres implantation. Fig. 9C showed that the CS/SF and CS/SF-HA groups expressed only a small amount of CD31, whereas the CS/Sr-SF-HA group expressed more CD31 (as indicated by the orange arrow), indicating more neovascularization.

At weeks 2, 4, and 8, the Masson staining results showed that the CS/Sr-SF-HA group had larger and darker blue stained areas than the CS/SF-HA group, and the CS/SF group had the lightest staining (Fig. 9D). This results indicated that the CS/Sr-SF-HA group had better collagen fibers regeneration and deposition than the CS/SF-HA and CS/SF groups. The H&E staining showed no obvious fibrous tissue formation or inflammatory infiltration. Therefore, the presence of a large collagen component might be attributed to osteogenesis [63].

In mature bone tissues, Osteocalcin (OCN) and type I collagen (COL-1) were highly expressed, so immunohistochemical staining was performed to illustrate COL-I and OCN expression in peri-implant tissues. OCN, a calcium-binding protein, is mainly synthesized by osteoblasts and plays an important role in regulating bone calcium metabolism [66]. COL-1 is the most important fibrous collagen component of the bone matrix during the osteogenic phase [67]. During extracellular matrix formation and maturation, COL-1 expression is a major manifestation of osteogenic differentiation [63,64]. As shown in Fig. 10, by analyzing images and semi-quantitative results, four weeks after microsphere implantation, it was observed that COL-1 and OCN expression was highest in the CS/SF-Sr-HA group (brown stained areas). Moreover, with increasing implantation time, COL-1 and OCN expression was higher in the CS/SF-HA and CS/Sr-SF-HA groups, whereas only limited COL-1 and OCN expression could be observed in the CS/SF group at 8 weeks post-operation. The results showed that the implantation of CS/Sr-SF-HA promoted ectopic osteogenesis *in vivo*, and the loading of strontium further increased the expression of COL-1 and OCN and enhanced osteogenesis differentiation [64]. This result was consistent with the results of cell experiments *in vitro*.

4. Conclusions

In this study, needle-shaped Sr-SF-HA were successfully "green" synthesized by hydrothermal co-precipitation using silk fibroin as an organic template. Then, Sr-SF-HA were successfully loaded on chitosan composite microspheres (CS/Sr-SF-HA) using the electrostatic spraying method. Statistical analysis showed that the diameter of CS/Sr-SF-HA was 409.4 ± 84.5 μm. CCK-8 assay and live/dead cell staining showed that CS/Sr-SF-HA had excellent biocompatibility. ALP staining and ARS assay showed that CS/Sr-SF-HA could effectively promote osteogenic differentiation of rBMSCs. Moreover, the results of qRT-PCR, western blotting, and immunofluorescence staining demonstrated that CS/Sr-SF-HA significantly promoted the expression of osteogenic genes (*OPN*, *RUNX2*, and *ALP*) and proteins (OPN, RUNX2) in rBMSCs. In addition, scratch assays, tubule formation tests, and qRT-PCR assays for angiogenesis-related genes (*VEGF*) showed that CS/Sr-SF-HA had potent angiogenic activity. *In vivo* experiments confirmed that CS/Sr-SF-HA could effectively promote angiogenesis and ectopic osteogenesis. In conclusion, CS/Sr-SF-HA, with excellent biocompatibility and improved angiogenic and osteogenic properties, has promising applications in the regeneration of bone defects.

CRediT authorship contribution statement

Yunfei Liu: Writing – original draft, Software, Methodology, Formal analysis, Data curation, Conceptualization. **Chengji Shi:** Writing – review & editing, Project administration, Methodology. **Piaoye Ming:** Writing – review & editing, Supervision, Methodology. **Lingling Yuan:** Writing – review & editing, Supervision, Methodology. **Xueyu Jiang:** Writing – review & editing, Supervision, Methodology. **Min Jiang:** Writing – review & editing, Supervision, Methodology. **Rui Cai:** Writing – review & editing, Methodology, Formal analysis, Data curation. **Xiaorong Lan:** Writing – review & editing, Supervision, Methodology. **Jingang Xiao:** Writing – review & editing, Supervision, Methodology, Funding acquisition, Formal analysis, Data curation, Conceptualization. **Gang Tao:** Writing – review & editing, Supervision, Methodology, Funding acquisition, Formal analysis, Data curation, Conceptualization.

Declaration of competing interest

The authors declare no conflict of interest. The founding sponsors had no role in the design of the study and in the decision to publish the results.

Data availability

Data will be made available on request.

Acknowledgements

This work was funded by the National Natural Science Foundation of China (82370938, 81870746), Special Project for Local Science and Technology Development Guided by the Central Government of Sichuan Province (2022ZYD0082), Project of Science & Technology Department of Sichuan Province (2022NSFSC0599), Sichuan Science and Technology Program (2022YFS0634), Luzhou Science and Technology Program (2023SYF101), Scientific Research Foundation of Southwest Medical University (2020ZRZD011), Key Program of Southwest Medical University (2021ZKZD009), Project of Stomatological Institute of Southwest Medical University (2021XJYJS01), Joint project of Luzhou Municipal People's Government and Southwest Medical University (2020LZXNYDZ09). Scientific Research Foundation of the Affiliated Stomatological Hospital of Southwest Medical University (2020QY02, 202007), and Southwest Medical University Affiliated Stomatological Hospital "Ruitai Nursery Fund" Research and Cultivation Program Project (2022RT02).

References

[1] R.F. Richter, C. Vater, M. Korn, T. Ahlfeld, M. Rauner, W. Pradel, B. Stadlinger, M. Gelinsky, A. Lode, P. Korn, Treatment of critical bone defects using calcium phosphate cement and mesoporous bioactive glass providing spatiotemporal drug delivery, Bioact. Mater. 28 (2023) 402–419.

[2] Y. Xia, X. Jing, X. Wu, P. Zhuang, X. Guo, H. Dai, 3D-printed dual-ion chronological release functional platform reconstructs neuro-vascularization network for critical-sized bone defect regeneration, Chem. Eng. J. 465 (2023) 143015.
[3] C. Li, F. Sun, J. Tian, J. Li, H. Sun, Y. Zhang, S. Guo, Y. Lin, X. Sun, Y. Zhao, Continuously released Zn^{2+} in 3D-printed PLGA/β-TCP/Zn scaffolds for bone defect repair by improving osteoinductive and anti-inflammatory properties, Bioact. Mater. 24 (2023) 361–375.
[4] S.-J. Jiang, M.-H. Wang, Z.-Y. Wang, H.-L. Gao, S.-M. Chen, Y.-H. Cong, L. Yang, S.-M. Wen, D.-D. Cheng, J.-C. He, S.-H. Yu, Radially porous nanocomposite scaffolds with enhanced capability for guiding bone regeneration in vivo, Adv. Funct. Mater. 32 (18) (2022) 2110931.
[5] Y. Chen, W. Sheng, J. Lin, C. Fang, J. Deng, P. Zhang, M. Zhou, P. Liu, J. Weng, F. Yu, D. Wang, B. Kang, H. Zeng, Magnesium oxide nanoparticle coordinated phosphate-functionalized chitosan injectable hydrogel for osteogenesis and angiogenesis in bone regeneration, ACS Appl. Mater. Interfaces 14 (6) (2022) 7592–7608.
[6] M.G. Burger, A. Grosso, P.S. Briquez, G.M.E. Born, A. Lunger, F. Schrenk, A. Todorov, V. Sacchi, J.A. Hubbell, D.J. Schaefer, A. Banfi, N. Di Maggio, Robust coupling of angiogenesis and osteogenesis by VEGF-decorated matrices for bone regeneration, Acta Biomater. 149 (2022) 111–125.
[7] S. Li, L. Zhang, C. Liu, J. Kim, K. Su, T. Chen, L. Zhao, X. Lu, H. Zhang, Y. Cui, X. Cui, F. Yuan, H. Pan, Spontaneous immunomodulation and regulation of angiogenesis and osteogenesis by Sr/Cu-borosilicate glass (BSG) bone cement to repair critical bone defects, Bioact. Mater. 23 (2023) 101–117.
[8] W. Sun, Y. Zhou, X. Zhang, W. Xia, Y. Xu, K. Lin, Injectable nano-structured silicon-containing hydroxyapatite microspheres with enhanced osteogenic differentiation and angiogenic factor expression, Ceram. Int. 44 (16) (2018) 20457–20464.
[9] D. Van hede, B. Liang, S. Anania, M. Barzegari, B. Verlée, G. Nolens, J. Pirson, L. Geris, F. Lambert, 3D-printed synthetic hydroxyapatite scaffold with in silico optimized macrostructure enhances bone formation in vivo, Adv. Funct. Mater. 32 (6) (2022) 2105002.
[10] Z. Fu, J. Cui, B. Zhao, S.G.F. Shen, K. Lin, An overview of polyester/hydroxyapatite composites for bone tissue repairing, Journal of Orthopaedic Translation 28 (2021) 118–130.
[11] X. Zhou, Y. Qian, L. Chen, T. Li, X. Sun, X. Ma, J. Wang, C. He, Flowerbed-inspired biomimetic scaffold with rapid internal tissue infiltration and vascularization capacity for bone repair, ACS Nano 17 (5) (2023) 5140–5156.
[12] D. Cheng, R. Ding, X. Jin, Y. Lu, W. Bao, Y. Zhao, S. Chen, C. Shen, Q. Yang, Y. Wang, Strontium ion-functionalized nano-hydroxyapatite/chitosan composite microspheres promote osteogenesis and angiogenesis for bone regeneration, ACS Appl. Mater. Interfaces 15 (16) (2023) 19951–19965.
[13] H. Yook, J. Hwang, W. Yeo, J. Bang, J. Kim, T.Y. Kim, J.-S. Choi, J.W. Han, Design strategies for hydroxyapatite-based materials to enhance their catalytic performance and applicability, Adv. Mater. 35 (2022) 2204938.
[14] K. Lin, P. Liu, L. Wei, Z. Zou, W. Zhang, Y. Qian, Y. Shen, J. Chang, Strontium substituted hydroxyapatite porous microspheres: surfactant-free hydrothermal synthesis, enhanced biological response and sustained drug release, Chem. Eng. J. 222 (2013) 49–59.
[15] M. Xing, Y. Jiang, W. Bi, L. Gao, Y.-L. Zhou, S.-L. Rao, L.-L. Ma, Z.-W. Zhang, H.-T. Yang, J. Chang, Strontium ions protect hearts against myocardial ischemia/reperfusion injury, Sci. Adv. 7 (3) (2021) eabe0726.
[16] N. Reznikov, M. Bilton, L. Lari, M.M. Stevens, R. Kröger, Fractal-like hierarchical organization of bone begins at the nanoscale, Science 360 (6388) (2018) eaao2189.
[17] L. Wang, J.L. Pathak, D. Liang, N. Zhong, H. Guan, M. Wan, G. Miao, Z. Li, L. Ge, Fabrication and characterization of strontium-hydroxyapatite/silk fibroin biocomposite nanospheres for bone-tissue engineering applications, Int. J. Biol. Macromol. 142 (2020) 366–375.
[18] T. Zhang, T. Tian, R. Zhou, S. Li, W. Ma, Y. Zhang, N. Liu, S. Shi, Q. Li, X. Xie, Y. Ge, M. Liu, Q. Zhang, S. Lin, X. Cai, Y. Lin, Design, fabrication and applications of tetrahedral DNA nanostructure-based multifunctional complexes in drug delivery and biomedical treatment, Nat. Protoc. 15 (8) (2020) 2728–2757.
[19] P. Ming, P. Rao, T. Wu, J. Yang, S. Lu, B. Yang, J. Xiao, G. Tao, Biomimetic Design and fabrication of sericin-hydroxyapatite based membranes with osteogenic activity for periodontal tissue regeneration, Front. Bioeng. Biotechnol. 10 (2022) 899293.
[20] M. Tavafoghi, M. Cerruti, The role of amino acids in hydroxyapatite mineralization, J. R. Soc. Interface 13 (123) (2016) 20160462.
[21] M. Yang, Y. Shuai, C. Zhang, Y. Chen, L. Zhu, C. Mao, H. OuYang, Biomimetic nucleation of hydroxyapatite crystals mediated by antheraea pernyi silk sericin promotes osteogenic differentiation of human bone marrow derived mesenchymal stem cells, Biomacromolecules 15 (4) (2014) 1185–1193.
[22] J. Huang, C. Wong, A. George, D.L. Kaplan, The effect of genetically engineered spider silk-dentin matrix protein 1 chimeric protein on hydroxyapatite nucleation, Biomaterials 28 (14) (2007) 2358–2367.
[23] Y. Liu, T. Zhang, M. Li, Z. Ouyang, F. Gao, C. Liu, C. Li, D. Liu, Z. Zhou, PLGA hybrid porous microspheres as human periodontal ligament stem cell delivery carriers for periodontal regeneration, Chem. Eng. J. 420 (2021) 129703.
[24] Y. Zhang, R. Sheng, J. Chen, H. Wang, Y. Zhu, Z. Cao, X. Zhao, Z. Wang, C. Liu, Z. Chen, P. Zhang, B. Kuang, H. Zheng, C. Shen, Q. Yao, W. Zhang, Silk fibroin and sericin differentially potentiate the paracrine and regenerative functions of stem cells through multiomics analysis, Adv. Mater. 35 (20) (2023) 2210517.
[25] L. Nie, H. Zhang, A. Ren, Y. Li, G. Fu, R.D. Cannon, P. Ji, X. Wu, S. Yang, Nano-hydroxyapatite mineralized silk fibroin porous scaffold for tooth extraction site preservation, Dent. Mater. 35 (10) (2019) 1397–1407.
[26] Y. Zhu, Y. Chen, G. Xu, X. Ye, D. He, J. Zhong, Micropattern of nano-hydroxyapatite/silk fibroin composite onto Ti alloy surface via template-assisted electrostatic spray deposition, Mater. Sci. Eng. C 32 (2) (2012) 390–394.
[27] W. Shao, J. He, F. Sang, B. Ding, L. Chen, S. Cui, K. Li, Q. Han, W. Tan, Coaxial electrospun aligned tussah silk fibroin nanostructured fiber scaffolds embedded with hydroxyapatite–tussah silk fibroin nanoparticles for bone tissue engineering, Mater. Sci. Eng. C 58 (2016) 342–351.
[28] L. Ma, Y. Sun, Q. Cheng, Z. Yang, J. Wang, Z. Xu, M. Yang, Y. Shuai, Silk protein-mediated biomineralization: from bioinspired strategies and advanced functions to biomedical applications, ACS Appl. Mater. Interfaces 15 (28) (2023) 33191–33206.
[29] M. Hussain, J. Xie, Z. Hou, K. Shezad, J. Xu, K. Wang, Y. Gao, L. Shen, J. Zhu, Regulation of drug release by tuning surface textures of biodegradable polymer microparticles, ACS Appl. Mater. Interfaces 9 (16) (2017) 14391–14400.
[30] Z. Zhao, Z. Wang, G. Li, Z. Cai, J. Wu, L. Wang, L. Deng, M. Cai, W. Cui, Injectable microfluidic hydrogel microspheres for cell and drug delivery, Adv. Funct. Mater. 31 (31) (2021) 2103339.
[31] Q. Li, B. Chang, H. Dong, X. Liu, Functional microspheres for tissue regeneration, Bioact. Mater. 25 (2023) 485–499.
[32] T. Xu, Y. Yang, D. Suo, H.P. Bei, X. Xu, X. Zhao, Electrosprayed regeneration-enhancer-element microspheres power osteogenesis and angiogenesis coupling, Small 18 (36) (2022) 2200314.
[33] Y. Sun, X. Chi, H. Meng, M. Ma, J. Wang, Z. Feng, Q. Quan, G. Liu, Y. Wang, Y. Xie, Y. Zheng, J. Peng, Polylysine-decorated macroporous microcarriers laden with adipose-derived stem cells promote nerve regeneration in vivo, Bioact. Mater. 6 (11) (2021) 3987–3998.
[34] J. Wu, G. Li, T. Ye, G. Lu, R. Li, L. Deng, L. Wang, M. Cai, W. Cui, Stem cell-laden injectable hydrogel microspheres for cancellous bone regeneration, Chem. Eng. J. 393 (2020) 124715.
[35] X. Peng, K. Dong, Y. Zhang, L. Wang, C. Wei, T. Lv, Z.L. Wang, Z. Wu, Sweat-permeable, biodegradable, transparent and self-powered chitosan-based electronic skin with ultrathin elastic gold nanofibers, Adv. Funct. Mater. 32 (20) (2022) 2112241.
[36] B. Fu, Q. Liu, M. Liu, X. Chen, H. Lin, Z. Zheng, J. Zhu, C. Dai, X. Dong, D.-P. Yang, Carbon dots enhanced gelatin/chitosan bio-nanocomposite packaging film for perishable foods, Chin. Chem. Lett. 33 (10) (2022) 4577–4582.
[37] F. Dai, J. Huang, W. Liao, D. Li, Y. Wu, J. Huang, Y. Long, M. Yuan, W. Xiang, F. Tao, Y. Cheng, H. Deng, Chitosan-TiO2 microparticles LBL immobilized nanofibrous mats via electrospraying for antibacterial applications, Int. J. Biol. Macromol. 135 (2019) 233–239.
[38] M. Jiang, S. Li, P. Ming, Y. Guo, L. Yuan, X. Jiang, Y. Liu, J. Chen, D. Xia, Y. He, G. Tao, Rational design of porous structure-based sodium alginate/chitosan sponges loaded with green synthesized hybrid antibacterial agents for infected wound healing, Int. J. Biol. Macromol. 237 (2023) 123944.
[39] D. López Barreiro, Z. Martín-Moldes, A. Blanco Fernández, V. Fitzpatrick, D. L. Kaplan, M.J. Buehler, Molecular simulations of the interfacial properties in silk–hydroxyapatite composites, Nanoscale 14 (30) (2022) 10929–10939.
[40] Z. Ding, Z. Fan, X. Huang, Q. Lu, W. Xu, D.L. Kaplan, Silk–hydroxyapatite nanoscale scaffolds with programmable growth factor delivery for bone repair, ACS Appl. Mater. Interfaces 8 (37) (2016) 24463–24470.
[41] J. Zheng, F. Wu, H. Li, M. Liu, Preparation of bioactive hydroxyapatite@halloysite and its effect on MC3T3-E1 osteogenic differentiation of chitosan film, Mater. Sci. Eng. C 105 (2019) 110072.
[42] P. Xia, K. Zhang, S. Yan, G. Li, J. Yin, Biomimetic, biodegradable, and osteoinductive microgels with open porous structure and excellent injectability for construction of microtissues for bone tissue engineering, Chem. Eng. J. 414 (2021) 128714.
[43] J. Wu, F. Liu, C. Chen, Z. Zhao, Y. Du, X. Shi, Y. Wu, H. Deng, Long-term antibacterial activity by synergistic release of biosafe lysozyme and chitosan from LBL-structured nanofibers, Carbohydr. Polym. 312 (2023) 120791.
[44] H.-W. Kim, Y.-J. Kim, Fabrication of strontium-substituted hydroxyapatite scaffolds using 3D printing for enhanced bone regeneration, J. Mater. Sci. 56 (2) (2021) 1673–1684.
[45] I. Ullah, M.A. Siddiqui, S.K. Kolawole, H. Liu, J. Zhang, L. Ren, K. Yang, Synthesis, characterization and in vitro evaluation of zinc and strontium binary doped hydroxyapatite for biomedical application, Ceram. Int. 46 (10) (2020) 14448–14459. Part A).
[46] B. Wang, Y. Li, S. Wang, F. Jia, A. Bian, K. Wang, L. Xie, K. Yan, H. Qiao, H. Lin, J. Lan, Y. Huang, Electrodeposited dopamine/strontium-doped hydroxyapatite composite coating on pure zinc for anti-corrosion, antimicrobial and osteogenesis, Mater. Sci. Eng. C 129 (2021) 112387.
[47] P. Makkar, H.J. Kang, A.R. Padalhin, O. Faruq, B. Lee, In-vitro and in-vivo evaluation of strontium doped calcium phosphate coatings on biodegradable magnesium alloy for bone applications, Appl. Surf. Sci. 510 (2020) 145333.
[48] L. Cheng, H. Wu, J. Li, H. Zhao, L. Wang, Polydopamine modified ultrathin hydroxyapatite nanosheets for anti-corrosion reinforcement in polymeric coatings, Corrosion Sci. 178 (2021) 109064.
[49] L. Chen, Q. Li, X. Wang, J. Zhang, G. Xu, X. Cao, J. Liu, F. Nan, W. He, Electrostatic spraying synthesis of energetic RDX@NGEC nanocomposites, Chem. Eng. J. 431 (2022) 133718.
[50] Y.-g. Bi, Z.-t. Lin, S.-t. Deng, Fabrication and characterization of hydroxyapatite/sodium alginate/chitosan composite microspheres for drug delivery and bone tissue engineering, Mater. Sci. Eng. C 100 (2019) 576–583.
[51] J. Li, Y. Lai, M. Li, X. Chen, M. Zhou, W. Wang, J. Li, W. Cui, G. Zhang, K. Wang, L. Liu, Y. Lin, Repair of infected bone defect with Clindamycin-Tetrahedral DNA nanostructure complex-loaded 3D bioprinted hybrid scaffold, Chem. Eng. J. 435 (2022) 134855.

[52] D. Li, X. Dong, X. Liu, H. Lin, D. Yang, X. Shi, C. Chen, F. Tao, L. Jiang, H. Deng, Cellulose nanofibers embedded chitosan/tannin hydrogel with high antibacterial activity and hemostatic ability for drug-resistant bacterial infected wound healing, Carbohydr. Polym. 329 (2024) 121687.
[53] L. Yuan, X. Jiang, M. Jiang, Y. Guo, Y. Liu, P. Ming, S. Li, P. Zhou, R. Cai, K. Yu, G. Tao, Biocompatible gellan gum/sericin hydrogels containing halloysite@polydopamine nanotubes with hemostasis and photothermal antibacterial properties for promoting infectious wound repair, Mater. Des. 227 (2023) 111744.
[54] L. Mao, L. Xia, J. Chang, J. Liu, L. Jiang, C. Wu, B. Fang, The synergistic effects of Sr and Si bioactive ions on osteogenesis, osteoclastogenesis and angiogenesis for osteoporotic bone regeneration, Acta Biomater. 61 (2017) 217–232.
[55] Y. Wu, T. Chang, W. Chen, X. Wang, J. Li, Y. Chen, Y. Yu, Z. Shen, Q. Yu, Y. Zhang, Release of VEGF and BMP9 from injectable alginate based composite hydrogel for treatment of myocardial infarction, Bioact. Mater. 6 (2) (2021) 520–528.
[56] R. Chen, D. Wen, W. Fu, L. Xing, L. Ma, Y. Liu, H. Li, C. You, Y. Lin, Treatment effect of DNA framework nucleic acids on diffuse microvascular endothelial cell injury after subarachnoid hemorrhage, Cell Prolif. 55 (4) (2022) e13206.
[57] X. Wu, Z. Tang, K. Wu, Y. Bai, X. Lin, H. Yang, Q. Yang, Z. Wang, X. Ni, H. Liu, L. Yang, Strontium–calcium phosphate hybrid cement with enhanced osteogenic and angiogenic properties for vascularised bone regeneration, J. Mater. Chem. B 9 (30) (2021) 5982–5997.
[58] X. Shao, Z. Hu, Y. Zhan, W. Ma, L. Quan, Y. Lin, MiR-26a-tetrahedral framework nucleic acids mediated osteogenesis of adipose-derived mesenchymal stem cells, Cell Prolif. 55 (7) (2022) e13272.
[59] L. Xia, Y. Xie, B. Fang, X. Wang, K. Lin, In situ modulation of crystallinity and nanostructures to enhance the stability and osseointegration of hydroxyapatite coatings on Ti-6Al-4V implants, Chem. Eng. J. 347 (2018) 711–720.
[60] U. Krause, A. Seckinger, C.A. Gregory, Assays of osteogenic differentiation by cultured human mesenchymal stem cells, Methods Mol. Biol. 698 (2011) 215–230.
[61] X. Guo, S. Wei, M. Lu, Z. Shao, J. Lu, L. Xia, K. Lin, D. Zou, Dose-dependent effects of strontium ranelate on ovariectomy rat bone marrow mesenchymal stem cells and human umbilical vein endothelial cells, Int. J. Biol. Sci. 12 (12) (2016) 1511–1522.
[62] L. Bai, M. Feng, Q. Li, Y. Zhao, G. Zhang, Z. Cai, J. Xiao, Y. Lin, Curcumin delivery using tetrahedral framework nucleic acids enhances bone regeneration in osteoporotic rats, Chem. Eng. J. 472 (2023) 144978.
[63] P. Wei, Z. Yuan, W. Jing, Y. Huang, Q. Cai, B. Guan, Z. Liu, X. Zhang, J. Mao, D. Chen, X. Yang, Strengthening the potential of biomineralized microspheres in enhancing osteogenesis via incorporating alendronate, Chem. Eng. J. 368 (2019) 577–588.
[64] P. Wei, W. Jing, Z. Yuan, Y. Huang, B. Guan, W. Zhang, X. Zhang, J. Mao, Q. Cai, D. Chen, X. Yang, Vancomycin- and strontium-loaded microspheres with multifunctional activities against bacteria, in angiogenesis, and in osteogenesis for enhancing infected bone regeneration, ACS Appl. Mater. Interfaces 11 (34) (2019) 30596–30609.
[65] W. Hou, J. Guo, J. Liu, Y. Zhao, W. Wei, D. Shu, H. Dai, Calcium-magnesium phosphate biphasic microspheres with nutrient microchannels promote angiogenesis and osteogenic differentiation, Mater. Des. 219 (2022) 110767.
[66] Y. Han, X. You, W. Xing, Z. Zhang, W. Zou, Paracrine and endocrine actions of bone—the functions of secretory proteins from osteoblasts, osteocytes, and osteoclasts, Bone Research 6 (1) (2018) 16.
[67] P. Gupta, M. Adhikary, J.C. M, M. Kumar, N. Bhardwaj, B.B. Mandal, Biomimetic, osteoconductive non-mulberry silk fiber reinforced tricomposite scaffolds for bone tissue engineering, ACS Appl. Mater. Interfaces 8 (45) (2016) 30797–30810.